AGU PUBLICATIONS

JGR

Journal of Geophysical Research: Space Physics

RESEARCH ARTICLE
10.1002/2015JA021487

On the origin of magnetosheath plasmoids and their relation to magnetosheath jets

T. Karlsson[1], A. Kullen[1], E. Liljeblad[1], N. Brenning[1], H. Nilsson[2], H. Gunell[3], and M. Hamrin[4]

[1]Space and Plasma Physics, School of Electrical Engineering, KTH Royal Institute of Technology, Stockholm, Sweden, [2]Swedish Institute of Space Physics, Kiruna, Sweden, [3]Belgian Institute for Space Aeronomy, Brussels, Belgium, [4]Department of Physics, Umeå University, Umeå, Sweden

Key Points:
- There are two populations of magnetosheath plasmoids, with different magnetic field signatures
- One population originates in the solar wind, the other is likely generated at the bow shock
- The latter population can be considered as a subset of magnetosheath jets, reported on recently

Correspondence to:
T. Karlsson,
tomas.karlsson@ee.kth.se

Citation:
Karlsson, T., A. Kullen, E. Liljeblad, N. Brenning, H. Nilsson, H. Gunell, and M. Hamrin (2015), On the origin of magnetosheath plasmoids and their relation to magnetosheath jets, *J. Geophys. Res. Space Physics*, *120*, 7390–7403, doi:10.1002/2015JA021487.

Received 22 MAY 2015
Accepted 12 AUG 2015
Accepted article online 15 AUG 2015
Published online 17 SEP 2015

Abstract We investigate localized magnetosheath and solar wind density enhancements, associated with clear magnetic field changes, and therefore referred to as magnetosheath/solar wind plasmoids, respectively. Using Cluster data, we show that there are two distinct populations of magnetosheath plasmoids, one associated with a decrease of magnetic field strength (diamagnetic plasmoids), and one with an increased magnetic field strength (paramagnetic plasmoids). The diamagnetic magnetosheath plasmoids have scale sizes of the order of 1–10 R_E, while the paramagnetic ones are an order of magnitude smaller. The diamagnetic plasmoids are not associated with any change in the magnetosheath plasma flow velocity, and they are classified as embedded plasmoids in the terminology of Karlsson et al. (2012). The paramagnetic plasmoids may either be embedded or associated with increases in flow velocity (fast plasmoids). A search for plasmoids in the pristine solar wind resulted in identification of 62 diamagnetic plasmoids with very similar properties to the magnetosheath diamagnetic plasmoids, making it probable that the solar wind is the source of these structures. No paramagnetic plasmoids are found in the pristine solar wind, indicating that these are instead created at the bow shock or in the magnetosheath. We discuss the relation of the plasmoids to the phenomenon of magnetosheath jets, with which they have many properties in common, and suggest that the paramagnetic plasmoids can be regarded as a subset of these or a closely related phenomenon. We also discuss how the results from this study relate to theories addressing the formation of magnetosheath jets.

1. Introduction

The pristine solar wind does not interact directly with the geomagnetic field, rather it is first decelerated, compressed, and heated at the bow shock, forming the magnetosheath behind it. The large-scale properties of the magnetosheath, both pressure [e.g., *Lucek et al.*, 2005] and magnetic field orientation [*Lu et al.*, 2013, 2014], determine the position of the magnetopause. These properties change more or less continuously with distance from the dayside bow shock and on timescales of the varying solar wind input [e.g., *Lucek et al.*, 2005].

Recently, however, there has been an interest in the presence of small-scale, transient increases in dynamic pressure (or equivalently, kinetic energy density) in the magnetosheath, which may locally affect the magnetopause. Such structures have been studied under several different designations: "magnetosheath dynamic pressure enhancements" [*Archer and Horbury*, 2013], "antisunward high-speed jets" [*Plaschke et al.*, 2013], "supermagnetosonic subsolar magnetosheath jets" [*Hietala et al.*, 2012], "transient flux enhancements" [*Němeček et al.*, 1998], "high kinetic energy density plasma jets" [*Savin et al.*, 2008], and "super fast plasma streams" [*Savin et al.*, 2012]. In this paper we will simply call the structures described in these and related papers "magnetosheath jets."

Magnetosheath jets have been shown to have considerable impact on the magnetopause, where their surplus momentum may cause severe local deformations of the magnetopause [*Amata et al.*, 2011; *Shue et al.*, 2009]. These deformations may launch surface [*Dmitriev and Suvorova*, 2012; *Archer et al.*, 2012] or compressional waves [*Plaschke et al.*, 2009], initiate ionospheric flow enhancements [*Hietala et al.*, 2012], and possibly penetrate directly into the magnetosphere [*Savin et al.*, 2012]. The increase in dynamic pressure of the magnetosheath jets has been reported to be due to either an increase in flow velocity [*Archer et al.*, 2012], in density [*Němeček et al.*, 1998; *Savin et al.*, 2008; *Archer and Horbury*, 2013; *Plaschke et al.*, 2013], or in both [*Amata et al.*, 2011; *Archer and Horbury*, 2013]. A generation mechanism for magnetosheath jets has not been agreed upon,

but they are generally believed to be formed at the bow shock, mainly during times of a radially directed interplanetary magnetic field [*Hietala et al.*, 2012; *Archer and Horbury*, 2013; *Hietala and Plaschke*, 2013; *Plaschke et al.*, 2013].

Meanwhile, small-scale variations in the magnetosheath have been studied from a slightly different point of view, in the form of localized density enhancements without any a priori connection to an increase in the flow velocity. *Hubert and Harvey* [2000] reported on transient density enhancements with an increase of 35% over the background density and concluded that they can enter the magnetosphere via the mechanism of impulsive penetration [e.g., *Lemaire*, 1977; *Echim and Lemaire*, 2000]. *Karlsson et al.* [2012] studied 56 localized structures where the density was at least 50% higher than that of the surrounding plasma. They concluded that all such structures were associated with some type of magnetic field change (rotation, increase, or decrease), and they were therefore termed plasmoids, following *Bostick* [1956]. We will use this terminology in the present paper. A majority of the plasmoids studied by *Karlsson et al.* [2012] were convecting with the background magnetosheath flow. These plasmoids were referred to as embedded plasmoids. A nonnegligible minority of the magnetosheath plasmoids were associated with an increase in flow velocity of more than 10% and were termed fast plasmoids by *Karlsson et al.* [2012]. Studies by *Gunell et al.* [2012, 2014] identified further fast plasmoids and showed that they at times penetrate into the magnetosphere.

The generation of magnetosheath plasmoids has not been discussed, and it is not known if they are created at the bow shock or in the magnetosheath, or if they are present in the solar wind and convect through the bow shock [*Karlsson et al.*, 2012].

Since the plasmoids represent an increase of the local dynamic pressure even when they are not associated with an increase in velocity, they could be considered a special case of, or at least related to, magnetosheath jets, depending on the definition used for the jets. A comparison of the properties of the two phenomena is therefore of great interest. If they are related, they may also have the same or similar generation mechanisms.

The purpose of this paper is twofold. First, to investigate if plasmoids similar to those observed in the magnetosheath can be found already in the pristine solar wind and thereby establish whether the plasmoids are created there or rather at the bow shock and/or magnetosheath. If they are present in the solar wind, it would indicate that the plasmoids are not closely related to the magnetosheath jets. Second, we wish to further study the relation between the magnetosheath plasmoids and jets, by investigating and comparing some of their properties, such as scale sizes and magnetic signatures. (*Karlsson et al.* [2012] did not consider the nature of the magnetic variation associated with the plasmoids.) We will also discuss the consequences of this relation for possible models of the creation of plasmoids and magnetosheath jets.

2. Method

We use data from the following instruments on board the Cluster satellites: Electric Fields and Waves (EFW) [*Gustafsson et al.*, 1997], the Fluxgate Magnetometer (FGM) [*Balogh et al.*, 2001], and the Cluster Ion Spectrometry (CIS) High Energy Analyzer (HIA) [*Rème et al.*, 2001]. These instruments provide the quantities used in this study, namely, the spacecraft potential, the DC magnetic field, and the ion flow velocity and temperature, respectively. For the magnetosheath plasmoids, we will revisit the data set used by *Karlsson et al.* [2012]. For the search of solar wind plasmoids, we will identify times when the Cluster spacecraft are in the solar wind. With an apogee of 19.8 Earth radii (R_E), considerable time is spent in the solar wind during January to April each year. For this study, we investigate data from the years 2002 to 2006.

For the solar wind plasmoids search, we follow a similar procedure to that which was used to identify the magnetosheath plasmoids by *Karlsson et al.* [2012]. Identification of time intervals when the Cluster spacecraft are in the solar wind can readily be made by inspecting Cluster Quicklook plots (http://www.cluster.rl.ac.uk/csdsweb/) with particular emphasis on ion energy spectra, floating potential, and ion velocity. We only consider data temporally separated by at least 1 h from any indication of a transition between the magnetosheath and the solar wind. We also explicitly check for foreshock signatures and exclude times when such are present. The spacecraft potential is converted to number density by a standard calibration (A. Vaivads, private communication, 2010), based on a comparison with the plasma frequency determined by the WHISPER instrument [*Trotignon et al.*, 2003]. In contrast to how *Karlsson et al.* [2012] proceeded, we use the same calibration for all events and do not construct an individual calibration for each event. This introduces

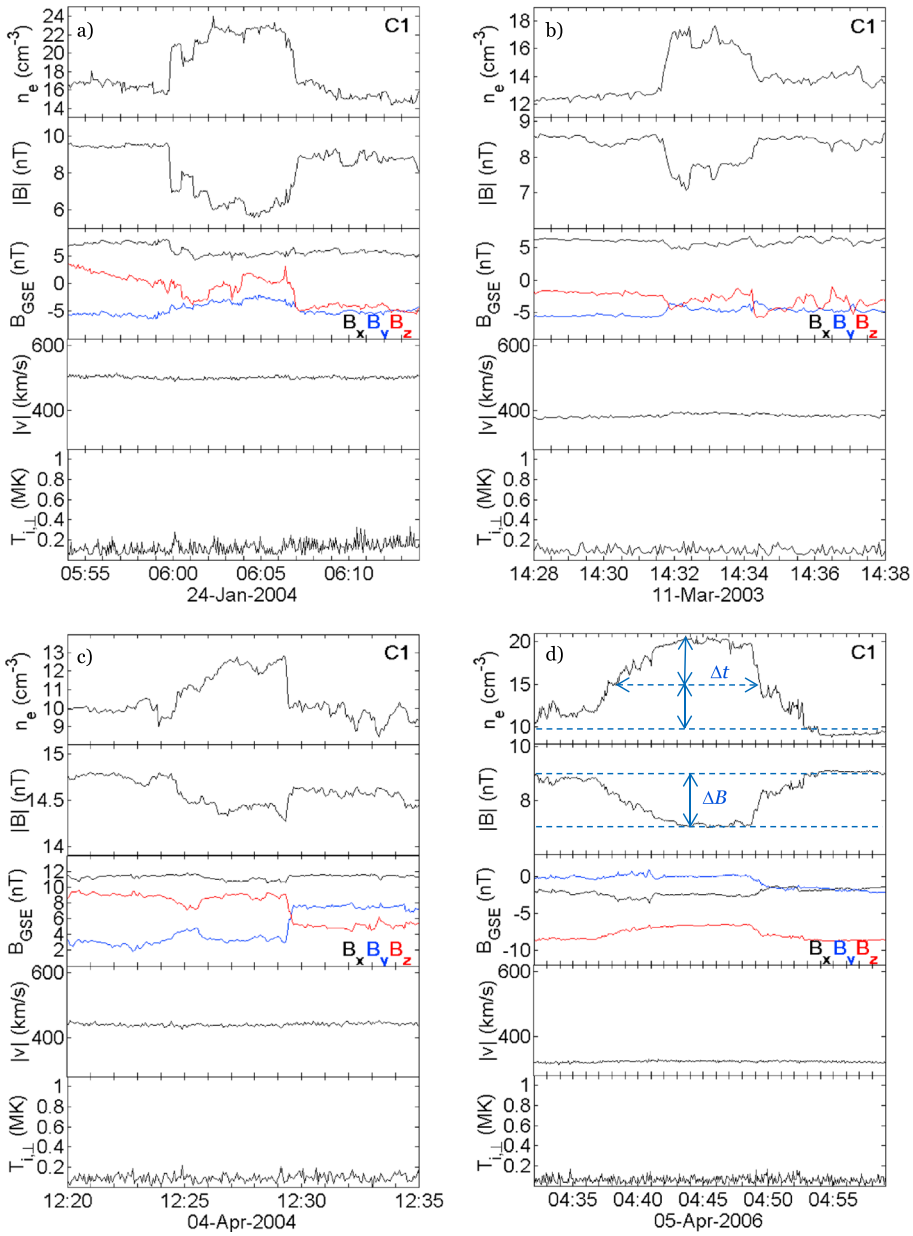

Figure 1. (a–d) Four examples of Cluster observations of solar wind plasmoids. From top to bottom the panels show electron density, total magnetic field, the three components of the magnetic field in GSE coordinates, the absolute value of the ion drift velocity, and the perpendicular ion temperature. All measurements presented are from Cluster 1 ("C1"). In Figure 1d the determination of the temporal scale Δt and the magnetic field change ΔB described in section 2 is exemplified.

some uncertainty in the absolute level of the densities, but since we are mainly interested in the variations in density, this procedure is quite sufficient.

In order to identify localized, isolated plasmoids we establish a background density by running a boxcar average with the same window width of 500 s as was used by *Karlsson et al.* [2012]. For a solar wind speed of 400 km/s, this corresponds to a spatial scale of 31 R_E. We then identify localized increases of the electron density over the background by a certain factor. *Karlsson et al.* [2012] set the lower limit at an increase of 50%. In the solar wind such a large increase turns out to be rather uncommon, and we have instead set the limit at 30%. Inspection of solar wind data from the years 2002 to 2006 resulted in the identification of 62 localized density enhancements. All of these were associated with clear magnetic field variations and are therefore in the following referred to as solar wind plasmoids. Figure 1 shows four examples of electron density, magnetic

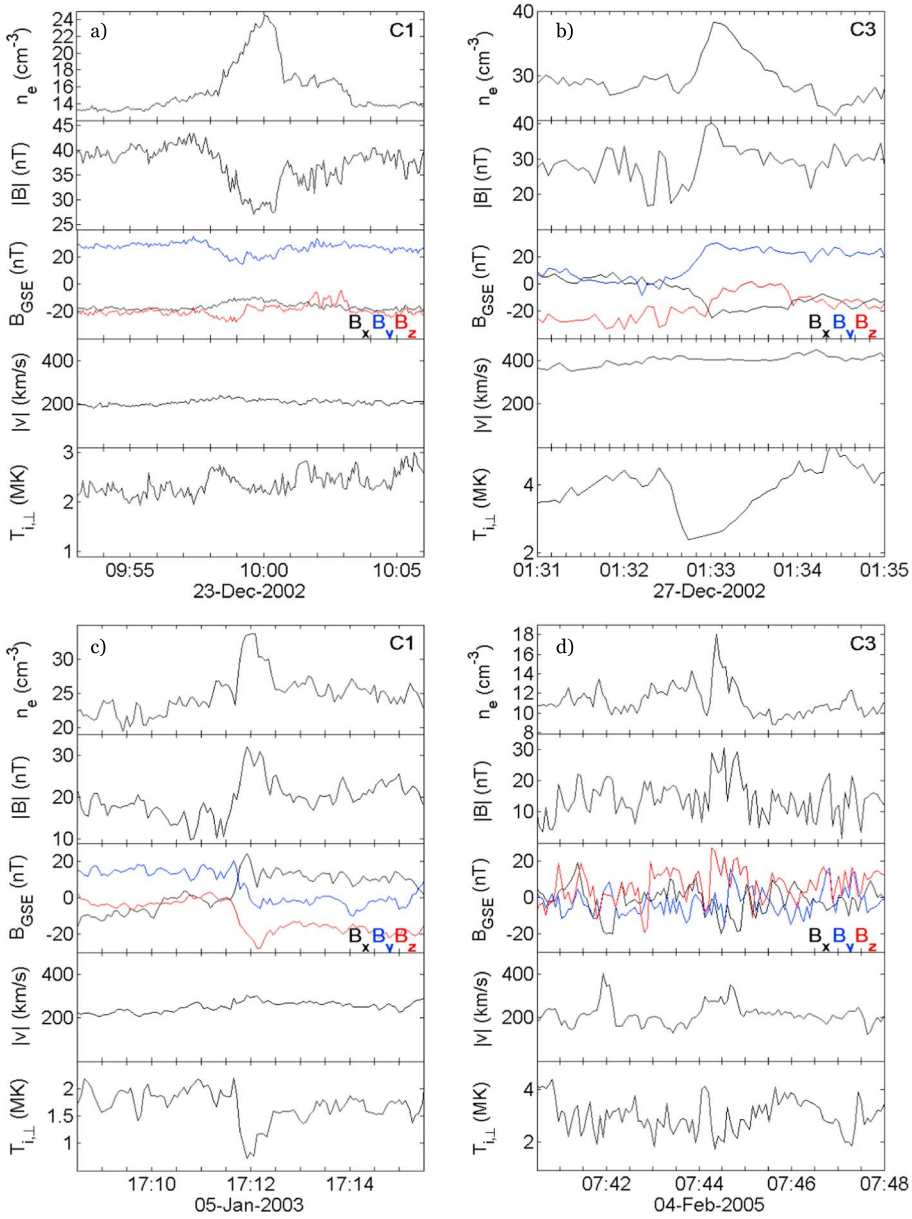

Figure 2. Four examples of magnetosheath plasmoids in the same format as in Figure 1. "C1" and "C3" indicate measurements from Cluster 1 and Cluster 3, respectively.

field, plasma flow velocity, and perpendicular ion temperature of typical solar wind plasmoids. All four events have a very similar appearance, with an anticorrelation between the density and magnetic field strength and with no change in the plasma flow velocity or perpendicular ion temperature associated with the plasmoids. (For the solar wind plasmoids presented in Figure 1, we have made an exception to our methodology and applied a manual calibration using WHISPER data from the same day according to the method described by *Karlsson et al.* [2012]).

For comparison, in Figure 2 we show four plasmoids from the magnetosheath, which were included in the study by *Karlsson et al.* [2012]. We can note that the magnetic field strength is generally higher for the magnetosheath cases, which is normal and due to compression of the solar wind as it crosses the bow shock and field line draping [e.g., *Lucek et al.*, 2005; *Coleman*, 2005]. The magnetosheath magnetic field is also more turbulent than the solar wind field [e.g., *Lucek et al.*, 2005].

Karlsson et al. [2012] did not consider the nature of the magnetic field signature associated with the magnetosheath plasmoids. Closer inspection shows that a large majority of the plasmoids are associated with either a clear increase of the total magnetic field (which we call a paramagnetic signature), or a clear decrease (diamagnetic signature). Figure 2a shows an example of a diamagnetic plasmoid. It is not associated with any clear change in velocity and therefore belongs to the category embedded plasmoids, as defined by *Karlsson et al.* [2012]. Figures 2b–2c show two examples of embedded plasmoids with a paramagnetic signature, whereas Figure 2d is an example of a fast plasmoid, also with a paramagnetic signature.

We have included, in total, 53 magnetosheath plasmoids from *Karlsson et al.* [2012] in this study. (Three plasmoid observations were discarded, since they had a complex morphology making it difficult to clearly define a scale size and magnetic field signature.) For the solar wind, no plasmoid was associated with a change in the ion flow velocity greater than 10%, and using the terminology applied to the magnetosheath, we may classify all solar wind plasmoids as embedded.

To compare the magnetosheath and solar wind plasmoids, we determine a quantitative measure of the magnetic field signature as indicated in Figure 1d: we manually determine a background level of the magnetic field strength B_{BG}, by averaging over regions of quiet magnetic field, typically 5–10 min before and after the plasmoid observations. We then note the maximum deviation ΔB from this (with the sign included). The relative magnetic field change is then defined as $\Delta B/B_{BG}$. We also estimate the scale size of the plasmoids, by a simplified version of the method used by *Karlsson et al.* [2012]. We determine the temporal scale size Δt of the event in the spacecraft frame as the time during which the deviation in the density from the background (determined in s similar way as the magnetic field background) is greater than half the maximum deviation. (This is again illustrated in Figure 1d.) The temporal scale size corresponds to the time it takes for the structure to pass over the spacecraft, as it is convected by the solar wind or magnetosheath plasma flow. (The spacecraft velocity is negligible compared to the flow velocities.) We then multiply Δt by the average of the ion flow velocity v, measured by the CIS HIA instrument over the plasmoid. This product is an estimate of the scale size l of the plasmoid. We exclusively use data from spacecraft (S/C) 1 and 3 for these determinations, since the ion moments are not available on S/C 2, and the moments from the CIS CODIF instrument on S/C 4 are less reliable. Between S/C 1 and 3, we select the one which measures the largest maximum electron density for the plasmoid, since this is likely to correspond to measurements from a more central part of the plasmoid. (*Karlsson et al.* [2012] showed that for spacecraft separations up to 2 R_E one of the spacecraft at times is likely to pass relatively close to the center of the plasmoid, since it is flanked by observations of lower electron density on either side. Furthermore, the shortest scale size did not depend strongly on distance away from the center.) This simple method of determining scale sizes of course has larger uncertainties than the more detailed method of *Karlsson et al.* [2012], but is quite adequate for showing differences in order of magnitude of scale sizes of the different types of plasmoids. For each plasmoid observation, we also record the spacecraft position in the GSE coordinate system, the ion flow velocity averaged over the plasmoid, and the deviation in perpendicular ion temperature, defined analogously to the magnetic field deviation.

3. Results

In Figure 3 we show the magnetic field change $\Delta B/B_{BG}$ as a function of the scale size l. We indicate by different symbols the following plasmoid populations: solar wind plasmoids, fast magnetosheath plasmoids, and embedded magnetosheath plasmoids. The latter population is subdivided into plasmoids with positive and negative ΔB, i.e., paramagnetic and diamagnetic signatures, respectively, for consistency with later figures. (Two plasmoids with negligible change in magnetic field strength were arbitrarily classified as paramagnetic.) Figure 3 shows a number of clear results. First of all, we note that all solar wind plasmoids are associated with diamagnetic signatures. For the magnetosheath plasmoids, on the other hand, 72% are associated with a paramagnetic signature and the remaining 28% with a diamagnetic signature. No clear dependence of the amplitude on the type of magnetic signature or the scale size can be seen. Second, all fast plasmoids except one are associated with paramagnetic signatures, with a similar spread in magnitude as the embedded paramagnetic plasmoids. Third, the scale sizes of the paramagnetic plasmoids, both embedded and fast, are similar, as are the scale sizes of the solar wind and magnetosheath diamagnetic plasmoids.

In order to quantify this last observation, we plot the distributions of scale sizes for the different populations in Figure 4. In Figure 4a is shown the distributions for the solar wind plasmoids (dashed red line) and embedded diamagnetic magnetosheath plasmoids (dashed black line). Figure 4b shows the distributions for the fast

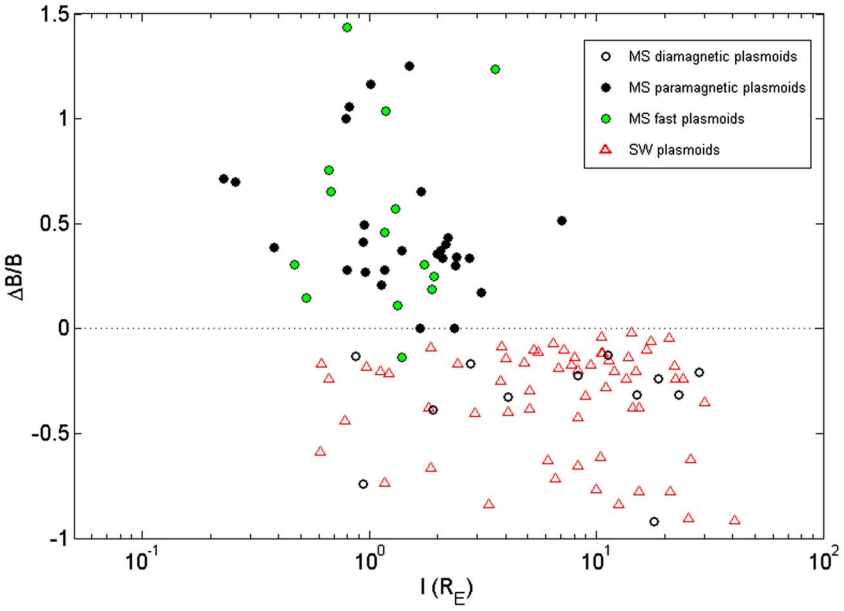

Figure 3. The relative change in magnetic field as a function of scale size *l* for all plasmoids. Solar wind (SW) plasmoids are represented by red triangles, together with the three different types of magnetosheath (MS) plasmoids: embedded diamagnetic plasmoids (unfilled circles), embedded paramagnetic plasmoids (black circles), and fast plasmoids (green circles).

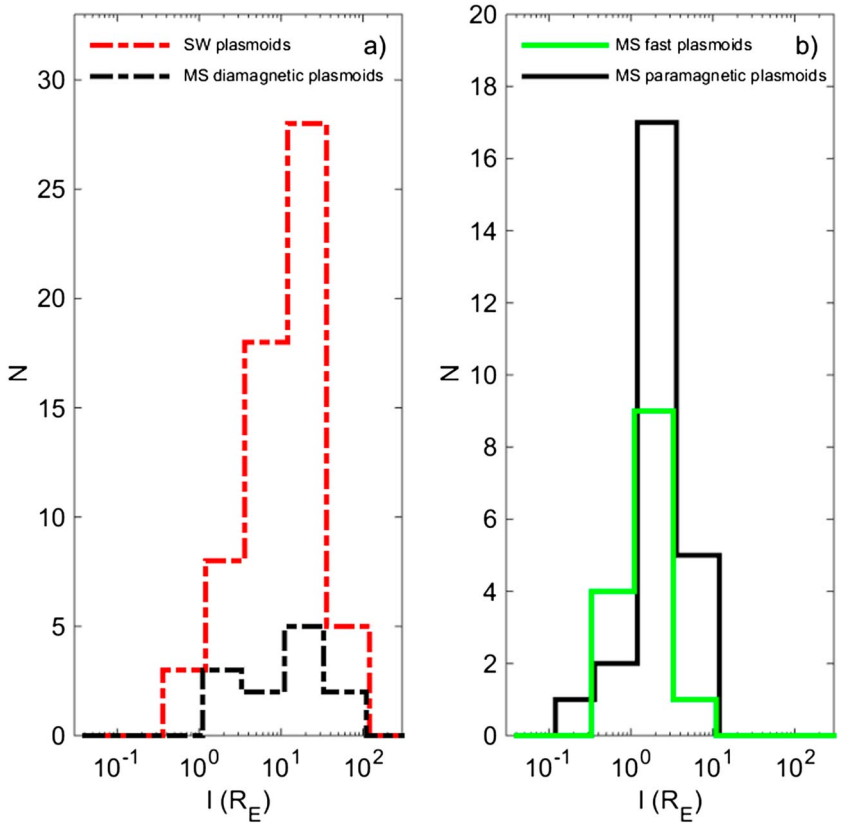

Figure 4. Distribution (number of found cases) of scale sizes for the different types of plasmoids. (a) The solar wind (SW) plasmoids (dashed red line) and embedded diamagnetic magnetosheath (MS) plasmoids (dashed black line). (b) The distributions for the fast magnetosheath plasmoids (solid green line) and paramagnetic embedded magnetosheath plasmoids (solid black line).

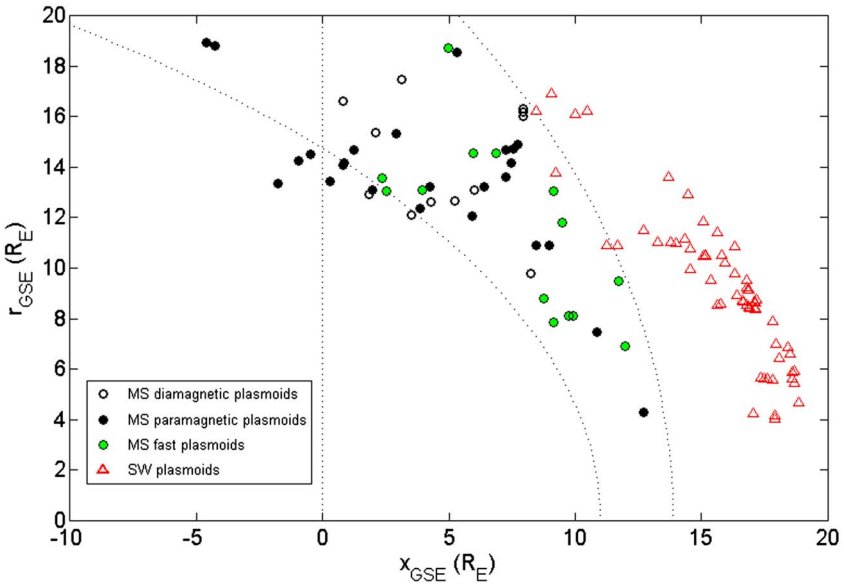

Figure 5. Position of different types of plasmoids in $x_{GSE} - r_{GSE}$ space, where $r_{GSE} = \sqrt{y_{GSE}^2 + z_{GSE}^2}$ is the distance from the x axis, using the same symbols as in Figure 3. Indicated are also the statistical magnetopause (for moderate solar wind pressure, [*Sibeck et al.*, 1991]) and magnetosheath [*Burgess*, 1995] positions.

magnetosheath plasmoids (solid green line) and embedded paramagnetic magnetosheath plasmoids (solid black line).

The distribution of solar wind plasmoids and embedded diamagnetic magnetosheath plasmoids are very similar with median scale sizes of 8.3 R_E and 9.8 R_E, respectively. Even after normalization to observation time, no reliable conclusions can be drawn from the amplitudes of the distributions, since a more strict criterion on density enhancement was placed on the magnetosheath plasmoids, as compared to the solar wind ones.

Also, the fast plasmoids and the embedded paramagnetic plasmoids have similar distributions, centered around scale sizes almost an order of magnitude lower than those of Figure 4a. The medians of the fast and embedded paramagnetic plasmoids are 1.2 R_E and 1.4 R_E, respectively. Since these two populations were found using the same data set and the same search criteria, we can take the difference in total number of

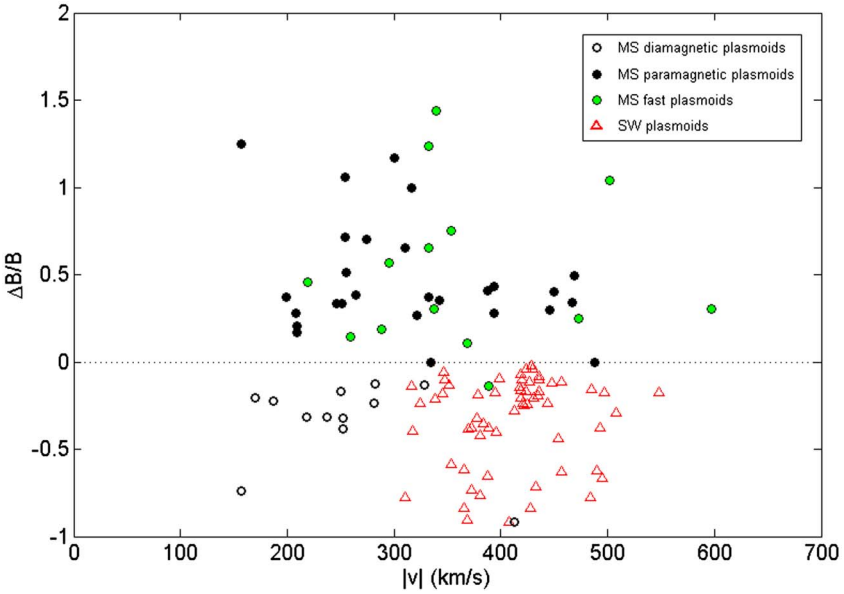

Figure 6. The relative change in magnetic field as a function of ion flow velocity, using the same symbols as in Figure 3.

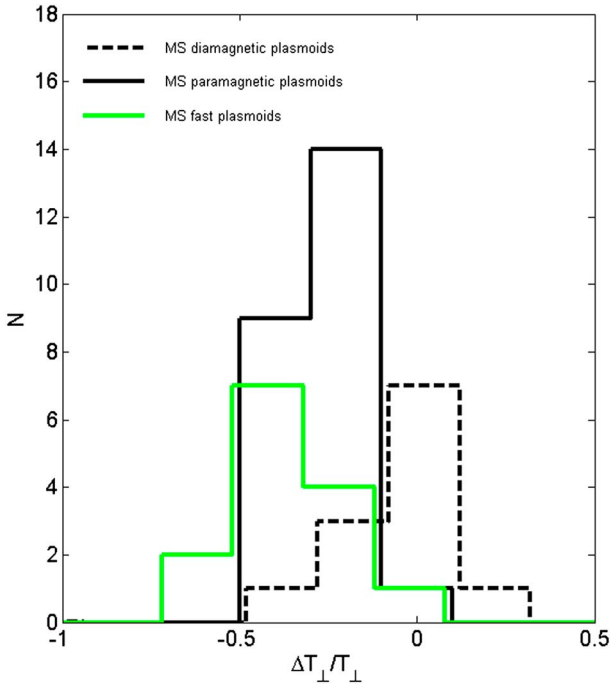

Figure 7. Distribution (number of found cases) of relative change in the perpendicular ion temperature for the different types of magnetosheath plasmoids. The color coding is the same as that in Figure 4.

identifications as an indication that the embedded plasmoids are more common than the fast ones, even if the statistics are limited.

The positions of all plasmoid observations are shown in Figure 5, in $x_{GSE} - r_{GSE}$ space, where $r_{GSE} = \sqrt{y_{GSE}^2 + z_{GSE}^2}$ is the distance from the x axis. Indicated are also the statistical magnetopause (for moderate solar wind pressure, [*Sibeck et al.*, 1991]) and magnetosheath [*Burgess*, 1995] positions. All plasmoid observations are relatively uniformly spread out over the regions sampled, but we can take note that the fast plasmoids are only observed for $x_{GSE} \gtrsim 2R_E$. Since the x coordinate of a plasmoid is a rough indication of the time it has spent in the magnetosheath, this is likely to indicate that the fast plasmoids brake down to the velocity of the surrounding magnetosheath plasma or that they impact on the magnetopause. The latter explanation would be consistent with the finding of *Karlsson et al.* [2012], who showed that the velocity vector of fast plasmoids was rotated toward the magnetopause, compared to that of the surrounding flow.

In Figure 6 we show the distribution of plasmoids in total plasma flow velocity and $\Delta B/B_{BG}$. Again, the fast and embedded paramagnetic plasmoids in the magnetosheath exhibit a very similar behavior, being present both for low-magnetosheath plasma flow velocities and quite high velocities. In contrast, the diamagnetic magnetosheath plasmoids are generally found for the lowest flow velocities. The solar wind plasmoids are evenly distributed for the typical solar wind speeds of 300–500 km/s.

Finally, Figure 7 shows the distribution of relative perpendicular ion temperature deviation from the surrounding plasma, for the three types of magnetosheath plasmoids, using the same color coding as in Figure 4. The solar wind plasmoids show no discernible signatures in the perpendicular ion temperature and are therefore not shown here. The diamagnetic, embedded plasmoids typically also show little temperature variation, whereas both types of paramagnetic plasmoids have a similar distribution, showing some perpendicular cooling.

Some of the plasmoid properties discussed in this section are summarized in Table 1.

4. Discussion

It is clear that there exist two distinct populations of magnetosheath plasmoids; one with a diamagnetic signature, with scale sizes of the order of 1 to a few tens of R_E, and one with a paramagnetic signature and an order of magnitude smaller scale sizes.

Table 1. Plasmoid Properties

		Magnetosheath		
	Solar Wind	Diamagnetic	Paramagnetic	Fast
Magnetic signature $\Delta B/B$	< 0	< 0	> 0	> 0
Fast/embedded	embedded	embedded	embedded	fast
Median scale size (R_E)	8.3	9.8	1.4	1.2
Ion temperature signature $\Delta T_\perp/T_\perp$	≈ 0	≈ 0	< 0	< 0

The diamagnetic magnetosheath plasmoids have very similar properties to the solar wind ones. Specifically, apart from the magnetic signature, they have a similar scale size distribution, and a lack of perpendicular ion cooling. Both the solar wind plasmoids and the diamagnetic magnetosheath plasmas are exclusively embedded in the surrounding plasma flow. Together, this suggests that the diamagnetic magnetosheath plasmoids originate from the solar wind plasmoids that cross the bow shock and convect downtail in the magnetosheath.

The solar wind plasmoids can likely be identified with structures reported on as "solar wind magnetic holes" or "solar wind magnetic decreases" [e.g., *Turner et al.*, 1977; *Tsurutani et al.*, 2011]. These are isolated decreases of the solar wind magnetic field with up to 80%, convecting with the solar wind speed and are associated with field-aligned increases of density, creating a pressure equilibrium structure [*Turner et al.*, 1977; *Burlaga and Lemaire*, 1978; *Stevens and Kasper*, 2007]. They have temporal scales, in the reference frame of the observing spacecraft, of a few seconds up to tens of minutes, which corresponds to spatial scales of a few hundred kilometers up to several tens of R_E. The upper cutoff in the distribution of Figure 4a is set by the size of the moving boxcar window, and the decrease at lower scale sizes may be related to the strict requirement on a density increase. In any case, the similar distributions between magnetosheath and solar wind diamagnetic signature strongly suggests that they are the same type of structure.

The relative density increase is typically greater in the magnetosheath plasmoids than in the solar wind ones. As discussed in section 2, we had to lower the criterion to a 30% increase in order to find a reasonable number of solar wind plasmoids. This is consistent with the results of *Grib and Leora* [2015], who modeled how a solar wind magnetic hole interacts with and passes through the bow shock. We have also checked that none of the properties of the plasmoids investigated here have a clear dependence on the relative density change of the plasmoids. We therefore conclude that lowering the limit for the relative density for the solar wind plasmoids, to study roughly the same number of events as for magnetosheath plasmoids is a valid approach.

No generation mechanism for solar wind magnetic holes has been agreed upon, but theories include Alfvén wave steepening at high-speed streams [*Tsurutani et al.*, 2002], compression [*Tsurutani et al.*, 2005], or wave-wave interaction [*Vasquez and Hollweg*, 1999] at corotating interaction regions, or the concept of magnetic mirror mode remnants [*Winterhalter et al.*, 1994]. They, however, also exist during times of quiet solar wind, without high-speed flows [*Xiao et al.*, 2014]. Possibly several generation mechanisms may be responsible, something that may be reflected in the fact that solar wind holes may be either "normal" or "linear," i.e., either associated with a magnetic field rotation or not across them [*Tsurutani et al.*, 2011].

In identifying the diamagnetic magnetosheath plasmoids with solar wind magnetic holes entering the magnetosheath via the bow shock, it may appear puzzling that their scale sizes are so similar. When passing the bow shock, any structure should be compressed when the solar wind flow is decelerated. The answer to this apparent inconsistency lies in the way the scale sizes are defined. In the simplified determination of the scale size used here, it is the dimension along the magnetosheath flow that is measured. Since the compressed plasmoids will be oriented according to the bow shock, as was shown by *Karlsson et al.* [2012], it is only close to the subsolar point that this will correspond to the shortest scale size of the plasmoid. At other positions in the magnetosheath the plasmoid will be oriented at some angle to the flow, and the spacecraft will sample a scale size which is greater than the shortest dimension of the plasmoid. To test this reasoning, we compare the scale sizes determined in this study to a more careful determination of the shortest scale size using a minimum variance method, performed by *Karlsson et al.* [2012]. The results can be seen in Figure 8, where open circles correspond to embedded paramagnetic plasmoids and filled circles to embedded paramagnetic plasmoids. For a majority of the plasmoids the shortest scale size determined by *Karlsson et al.* [2012] is smaller than the ones reported in this paper. A full multipoint study of solar wind plasmoids/magnetic holes is outside the scope of this paper but is an interesting future study. *Xiao et al.* [2010] argue that linear magnetic holes have an ellipsoidal shape, with an average major semiaxis of around 3 R_E and a minor semiaxis of around 1 R_E. For the normal magnetic holes, however, it is unclear if they have a similar shape or if their shape is modified during the transit of the bow shock, maybe producing smaller scales than were originally present in the solar wind. Further study is needed to resolve this question.

In contrast to the case of the diamagnetic plasmoids, for the paramagnetic magnetosheath plasmoids, we have found no analogous structures in the solar wind. The paramagnetic plasmoids (including both embedded and fast ones) are distributed equally over the whole of the magnetosheath (Figure 5), which points to a probable generation at the bow shock. Depending on the definition of magnetosheath jets, the embedded paramagnetic plasmoids may be considered a special case of the former. (*Archer et al.* [2012], for example,

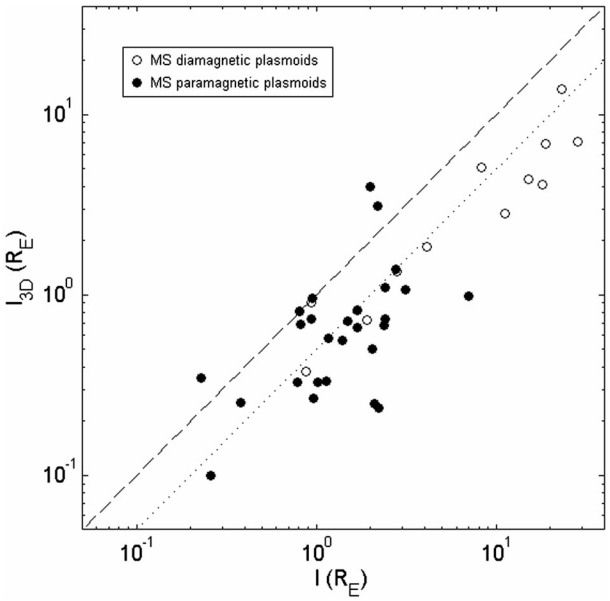

Figure 8. Scale size l_{3D} of magnetosheath (MS) plasmoids determined by the method used in *Karlsson et al.* [2012] as a function of scale size l determined in this study. Open circles correspond to embedded diamagnetic plasmoids and filled circles to embedded paramagnetic plasmoids. The dashed line shows $l_{3d} = l$ and the dotted line $l_{3d} = 0.5l$.

define the jets in terms of a jump in dynamic pressure of 1 nPa, whereas *Plaschke et al.* [2013] require an explicit increase in velocity.) The magnetosheath plasmoids certainly have many properties in common with magnetosheath jets. The latter have been reported by *Archer and Horbury* [2013] to have temporal scales in the spacecraft frame of 12–201 s, with a median of 34 s. For a typical flow speed of 200 km/s [*Archer et al.*, 2012], these correspond to spatial scales of 0.4, 6.3, and 1.1 R_E, respectively. *Savin et al.* [2008] report on an average scale size along the magnetosheath flow of 0.9 R_E, and *Plaschke et al.* [2013] give a median value of 0.6 R_E. These values are consistent with the distribution of paramagnetic plasmoid scale sizes reported here, both for embedded and fast ones. In contrast to the diamagnetic plasmoids, the paramagnetic ones are associated with lower perpendicular ion temperatures than those of the surrounding magnetosheath plasma (Figure 7). This behavior has also been found for magnetosheath jets associated with density enhancements [*Archer et al.*, 2012; *Archer and Horbury*, 2013; *Plaschke et al.*, 2013]. Paramagnetic plasmoids are found for a large spread of magnetosheath flow velocities, a behavior that is not observed for the diamagnetic magnetosheath plasmoids (Figure 6). This is again consistent with the properties of magnetosheath jets, which are often observed during times of high (even supermagnetosonic) general flow velocities in the magnetosheath [*Amata et al.*, 2011].

Magnetosheath jets have been reported to be associated with either an increase of the magnetic field [*Archer and Horbury*, 2013; *Plaschke et al.*, 2013], no correlation [*Němeček et al.*, 1998], or a decrease of the magnetic field [*Archer and Horbury*, 2013]. However, *Archer and Horbury* [2013] show that for jets where the density enhancement relative to the surrounding plasma is greater than 40%, the magnetic field signature is exclusively positive, consistent with the behavior of the paramagnetic plasmoids.

All these similarities between magnetosheath jets and paramagnetic magnetosheath plasmoids lead us to conclude that they are closely related. *Archer and Horbury* [2013] show that there is a distribution of jet events, where in one extreme they are associated with a pure velocity increase and no density increase, in the other extreme associated with the opposite behavior, and with a continuum in between. However, note that according to their definition of a minimum increase of 100% of the kinetic pressure for a jet, the embedded paramagnetic plasmoids typically do not fulfill the magnetosheath jet criterion. Instead, they can be seen as weaker, jet-like events. These would be located at the region of the distribution of magnetosheath jets which *Archer and Horbury* [2013] call purely density-driven enhancements, in their Figure 3a. (This was indeed hypothesized by the above authors.) Similarly, the fast plasmoids fit in well in the part of the distribution where the density and velocity enhancements both contribute to the enhancement in the dynamic pressure.

An unambiguous answer to the question of how magnetosheath jets and plasmoids are formed is not available, and it is outside the scope of this paper to provide it. We will, however, briefly discuss some of the proposed generation mechanisms for magnetosheath jets in the context of the present investigation.

Solar wind discontinuities have been suggested as one type of driver of magnetosheath jets, based on simulations of their interaction with the bow shock [*Lin et al.*, 1996; *Tsubouchi and Matsumoto*, 2005; *Archer et al.*, 2012]. These simulations, however, show a decrease of the magnetic field strength correlated with the increase in kinetic pressure and are not consistent with the paramagnetic plasmoids investigated here. *Archer and Horbury* [2013] demonstrated that some magnetosheath jets may be signatures of flux transfer events

[*Russell and Elphic*, 1979]. However, all these events were associated with a decrease in plasma density. *Savin et al.* [2008] suggest that the density enhancements are due to a pileup of magnetosheath plasma driven by magnetosheath jets. This seems unlikely in our case, since increases in density and magnetic field strength are seen for both embedded and fast plasmoids. Acceleration by a magnetic "slingshot effect" at times when coronal mass ejections interact with the near-Earth environment has been simulated by *Lavraud et al.* [2007]. They show that this can lead to localized regions of accelerated plasma within the magnetosheath. Their results, however, indicate that the velocities only become high downtail of Earth, which is not consistent with the fact that the fast plasmoids are exclusively observed for positive x_{GSE}. On the other hand, it is interesting to ask how jets and plasmoids are affected by local forces in the magnetosheath. *Karlsson et al.* [2015], using Cluster multipoint data, studied how magnetic and thermal pressure gradient forces locally accelerate or brake the plasma in bursty bulk flow events. A similar study performed on magnetosheath jets and plasmoids may yield interesting results on how these structures eventually will effect the magnetopause.

In a series of papers *Hietala et al.* [2009, 2012] and *Hietala and Plaschke*, [2013] suggest a mechanism for magnetosheath formation based on small-scale corrugations of the bow shock. These corrugations are possibly connected with SLAMS (short, large-amplitude magnetic structures) [*Schwartz and Burgess*, 1991] or as suggested by *Savin et al.* [2012] with hot flow anomalies (HFAs) [e.g., *Schwartz et al.*, 2000]. At the regions of such corrugations where the solar wind flow is almost tangential to the bow shock, the flow will cross the bow shock with almost no braking, in accordance with the Rankine-Hugoniot jump conditions [*Hietala et al.*, 2009]. This mechanism has been verified to some extent by simulations by *Karimabadi et al.* [2014] and the statistical study by *Plaschke et al.* [2013]. However, it is not clear how it can produce the distinct increases in density and magnetic field associated with the paramagnetic plasmoids. *Hietala and Plaschke* [2013] suggest that focusing of the flow or the interaction of two flow channels may produce this increase, but it is unclear why such increases would remain coherent structures far tailward of Earth.

This last observation touches on a general problem. The diamagnetic plasmoids can exist in a pressure balance between an increase of thermal pressure due to the increase in density and a decrease in magnetic pressure. For the paramagnetic plasmoids, no such pressure balance can exist. One possibility would be that the plasmoids are associated with fast mode solitons, as suggested by *Savin et al.* [2008]. They would then propagate with the fast magnetosonic phase velocity with respect to the magnetosheath plasma. This is, however, not consistent with the fact that the multispacecraft observations of the plasmoids line up very well, when transformed into the magnetosheath local plasma reference frame [*Karlsson et al.*, 2012], indicating that the plasmoids have a zero velocity in the plasma reference frame.

Archer et al. [2012] found SLAMS unlikely to be associated with magnetosheath jets. However, the paramagnetic plasmoids, both embedded and fast, have many properties in common with SLAMS, which are formed in the foreshock of the quasi-parallel bow shock by nonlinear interaction of ULF waves with reflected, energetic ions [*Schwartz*, 1991; *Scholer and Burgess*, 1992; *Giacalone et al.*, 1993]. Morphologically, SLAMS are isolated increases in magnetic field magnitude [e.g., *Schwartz*, 1991], correlated with an increase in plasma density [*Behlke et al.*, 2003]. They have scale sizes of the order of 0.1–1 R_E and are cooler than the magnetosheath plasma [*Schwartz et al.*, 1992]. Both simulations [*Dubouloz and Scholer*, 1995] and observations [*Lucek et al.*, 2008] have shown that they are likely to be oriented according to the overall bow shock orientation, similarly to what was found for magnetosheath plasmoids by *Karlsson et al.* [2012]. Upstream of the bow shock, their propagation speed in the plasma reference frame depends on their amplitude [*Schwartz et al.*, 1992], with smaller amplitude SLAMS having a small propagation speed. In fact, *Behlke et al.* [2003] have shown that SLAMS can move with the same velocity as the plasma and interpret this as a nonlinear trapping of the reflected ions [*Akimoto et al.*, 1991]. Furthermore, SLAMS have been proposed to penetrate the bow shock and convect into the terrestrial magnetosheath during certain circumstances [*Karimabadi et al.*, 2014]. The same process has also been reported in the Jovian magnetosheath [*Tsurutani et al.*, 1993]. It is tempting to suggest the following scenario: at times small-amplitude SLAMS will convect with the upstream plasma through the bow shock. The magnetosheath paramagnetic plasmoids would correspond to small-amplitude SLAMS, since the latter usually have an increase of the magnetic field of a factor of 2–3 to the surrounding field. These small-amplitude SLAMS will continue to convect with the magnetosheath flow, due to ion trapping [*Akimoto et al.*, 1991; *Behlke et al.*, 2003], keeping their identity due to their solitary wave nature. They can be identified with the embedded paramagnetic plasmoids of this study. Due to the abundance of SLAMS in the foreshock [*Schwartz*, 1991], once in a while a small-amplitude foreshock SLAMS may encounter a corrugation in the bow shock (due to either a large-amplitude SLAMS or an HFA) and cross the bow shock while maintaining a

velocity higher than that of the surrounding magnetosheath. This will result in a magnetosheath jet, with an additional increase in magnetic field strength and density. Such a structure could be identified with the fast paramagnetic plasmoids.

5. Conclusions

In conclusion, we suggest that magnetosheath plasmoids consist of two distinct populations, one with a diamagnetic signature and scale sizes of the order of 1–10 R_E, and one with a paramagnetic signature and an order of magnitude smaller scale sizes. The diamagnetic population is present already in the pristine solar wind, and we suggest that they are instances of magnetic holes, reported on earlier, that penetrate through the bow shock.

No paramagnetic plasmoids are found in the pristine solar wind, and they are therefore likely to be created at the bow shock. The fast paramagnetic magnetosheath plasmoids can be considered as a subpopulation of magnetosheath jets, with their increase in kinetic pressure and velocity. The embedded paramagnetic plasmoids can also be seen as either a subset or a generalization of magnetosheath jets, depending on the definition of the latter.

If the plasmoids are a subset of magnetosheath jets and have the same generation mechanism, this provides some clues that may exclude some of the proposed theories for jet generation, as discussed above. In this context, we have also discussed a possible connection between the paramagnetic plasmoids and the phenomenon of foreshock SLAMS.

Acknowledgments
We thank the EFW, CIS, FGM, and WHISPER teams, and the Cluster Science Archive (CSA). All data used in this study can be found at CSA (http://www.cosmos.esa.int/web/csa).

Yuming Wang thanks two anonymous reviewers for their assistance in evaluating this paper.

References

Akimoto, K., D. Winske, T. G. Onsager, M. F. Thomsen, and S. P. Gary (1991), Steepening of parallel propagating hydromagnetic waves into magnetic pulsations, *J. Geophys. Res.*, *96*, 17,599–17,607.

Amata, E., S. P. Savin, D. Ambrosino, Y. V. Bogdanova, M. F. Marcucci, S. Romanov, and A. Skalsky (2011), High kinetic energy density jets in the Earth's magnetosheath: A case study, *Planet. Space Sci.*, *59*, 482–494, doi:10.1016/j.pss.2010.07.021.

Archer, M. O., and T. S. Horbury (2013), Magnetosheath dynamic pressure enhancements: Occurrence and typical properties, *Ann. Geophys.*, *31*, 319–331, doi:10.5194/angeo-31-319-2013.

Archer, M. O., T. S. Horbury, and J. P. Eastwood (2012), Magnetosheath pressure pulses: Generation downstream of the bow shock from solar wind discontinuities, *J. Geophys. Res.*, *117*, A05228, doi:10.1029/2011JA017468.

Balogh, A., et al. (2001), The Cluster magnetic field investigation: Overview of in-flight performance and initial results, *Ann. Geophys.*, *19*, 1207–1217, doi:10.5194/angeo-19-1207-2001.

Behlke, R., M. André, S. C. Buchert, A. Vaivads, A. I. Eriksson, E. A. Lucek, and A. Balogh (2003), Multi-point electric field measurements of Short Large-Amplitude Magnetic Structures (SLAMS) at the Earth's quasi-parallel bow shock, *Geophys. Res. Lett.*, *30*(4), 1177, doi:10.1029/2002GL015871.

Bostick, W. H. (1956), Experimental study of ionized matter projected across a magnetic field, *Phys. Rev.*, *104*, 292–299.

Burgess, D. (1995), Collisionless shocks, in *Introduction to Space Physics*, edited by M. G. Kivelson and C. T. Russel, pp. 129–163, Cambridge Univ. Press, Cambridge, U. K.

Burlaga, L. F., and J. F. Lemaire (1978), Interplanetary magnetic holes: Theory, *J. Geophys. Res.*, *83*(A11), 5157–5160, doi:10.1029/JA083iA11p05157.

Coleman, I. J. (2005), A multi-spacecraft survey of magnetic field line draping in the dayside magnetosheath, *Ann. Geophys.*, *23*, 885–900, doi:10.5194/angeo-23-885-2005.

Dmitriev, A. V., and A. V. Suvorova (2012), Traveling magnetopause distortion related to a large-scale magnetosheath plasma jet: THEMIS and ground-based observations, *J. Geophys. Res.*, *117*, A08217, doi:10.1029/2011JA016861.

Dubouloz, N., and M. Scholer (1995), Two-dimensional simulations of magnetic pulsations upstream of the Earth's bow shock, *J. Geophys. Res.*, *100*, 9461–9474, doi:10.1029/94JA03239.

Echim, M. M., and J. F. Lemaire (2000), Laboratory and numerical simulations of the impulsive penetration mechanism, *Space Sci. Rev.*, *92*, 565–601, doi:10.1023/A:1005264212972.

Giacalone, J., S. J. Schwartz, and D. Burgess (1993), Observations of suprathermal ions in association with SLAMS, *Geophys. Res. Lett.*, *20*, 149–152.

Grib, S. A., and S. N. Leora (2015), The magnetic hole as plasma inhomogeneity in the solar wind and related interplanetary medium perturbations, *Geomagn. Aeron.*, *55*(2), 158–165.

Gunell, H., H. Nilsson, G. Stenberg, M. Hamrin, T. Karlsson, R. Maggiolo, M. Andreé, R. Lundin, and I. Dandouras (2012), Plasma penetration of the dayside magnetopause, *Phys. Plasmas*, *19*(7), 072906.

Gunell, H., et al. (2014), Waves in high-speed plasmoids in the magnetosheath and at the magnetopause, *Ann. Geophys.*, *32*(8), 991–1009.

Gustafsson, G., et al. (1997), The electric field and wave experiment for the Cluster mission, *Space Sci. Rev.*, *79*, 137–156, doi:10.1023/A:1004975108657.

Hietala, H., and F. Plaschke (2013), On the generation of magnetosheath high-speed jets by bow shock ripples, *J. Geophys. Res. Space Physics*, *118*, 7237–7245, doi:10.1002/2013JA019172.

Hietala, H., T. V. Laitinen, K. Andréeová, R. Vainio, A. Vaivads, M. Palmroth, T. I. Pulkkinen, H. E. J. Koskinen, E. A. Lucek, and H. Rème (2009), Supermagnetosonic jets behind a collisionless quasiparallel shock, *Phys. Rev. Lett.*, *103*, 245001, doi:10.1103/PhysRevLett.103.245001.

Hietala, H., N. Partamies, T. V. Laitinen, L. B. N. Clausen, G. Facskó, A. Vaivads, H. E. J. Koskinen, I. Dandouras, H. Rème, and E. A. Lucek (2012), Supermagnetosonic subsolar magnetosheath jets and their effects: From the solar wind to the ionospheric convection, *Ann. Geophys.*, *30*, 33–48, doi:10.5194/angeo-30-33-2012.

Hubert, D., and C. C. Harvey (2000), Interplanetary rotational discontinuities: From the solar wind to the magnetosphere through the magnetosheath, *Geophys. Res. Lett.*, *27*, 3149–3152, doi:10.1029/2000GL003776.

Karimabadi, H., et al. (2014), The link between shocks, turbulence, and magnetic reconnection in collisionless plasmas, *Phys. Plasmas*, *21*, 062308, doi:10.1063/1.4882875.

Karlsson, T., N. Brenning, H. Nilsson, J.-G. Trotignon, X. Vallières, and G. Facsko (2012), Localized density enhancements in the magnetosheath: Three-dimensional morphology and possible importance for impulsive penetration, *J. Geophys. Res.*, *117*, A03227, doi:10.1029/2011JA017059.

Karlsson, T., M. Hamrin, H. Nilsson, A. Kullen, and T. Pitkänen (2015), Magnetic forces associated with bursty bulk flows in Earth's magnetotail, *Geophys. Res. Lett.*, *42*, 3122–3128, doi:10.1002/2015GL063999.

Lavraud, B., J. E. Borovsky, A. J. Ridley, E. W. Pogue, M. F. Thomsen, H. Rème, A. N. Fazakerley, and E. A. Lucek (2007), Strong bulk plasma acceleration in Earth's magnetosheath: A magnetic slingshot effect?, *Geophys. Res. Lett.*, *34*, L14102, doi:10.1029/2007GL030024.

Lemaire, J. (1977), Impulsive penetration of filamentary plasma elements into the magnetospheres of the Earth and Jupiter, *Planet. Space Sci.*, *25*, 887–890, doi:10.1016/0032-0633(77)90042-3.

Lin, Y., L. C. Lee, and M. Yan (1996), Generation of dynamic pressure pulses downstream of the bow shock by variations in the interplanetary magnetic field orientation, *J. Geophys. Res.*, *101*, 479–493, doi:10.1029/95JA02985.

Lu, J. Y., Z.-Q. Liu, K. Kabin, H. Jing, M. X. Zhao, and Y. Wang (2013), The IMF dependence of the magnetopause from global MHD simulations, *J. Geophys. Res. Space Physics*, *118*, 3113–3125, doi:10.1029/2013JA018672.

Lu, J. Y., M. Wang, K. Kabin, J. S. Zhao, Z.-Q. Liu, M. X. Zhao, and G. Li (2014), Pressure balance across the magnetopause: Global MHD results, *Planet. Space Sci.*, *106*, 108–115, doi:10.1016/j.pss.2014.12.003.

Lucek, E. A., D. Constantinescu, M. L. Goldstein, J. Pickett, J. L. Pinçon, F. Sahraoui, R. A. Treumann, and S. N. Walker (2005), The magnetosheath, *Space Sci. Rev.*, *118*, 95–152.

Lucek, E. A., T. S. Horbury, I. Dandouras, and H. Rème (2008), Cluster observations of the Earth's quasi-parallel bow shock, *J. Geophys. Res.*, *113*, A07S02, doi:10.1029/2007JA012756.

Němeček, Z., J. Šafránková, L. Přech, D. G. Sibeck, S. Kokubun, and T. Mukai (1998), Transient flux enhancements in the magnetosheath, *Geophys. Res. Lett.*, *25*, 1273–1276, doi:10.1029/98GL50873.

Plaschke, F., K.-H. Glassmeier, H. U. Auster, O. D. Constantinescu, W. Magnes, V. Angelopoulos, D. G. Sibeck, and J. P. McFadden (2009), Standing Alfvén waves at the magnetopause, *Geophys. Res. Lett.*, *36*, L02104, doi:10.1029/2008GL036411.

Plaschke, F., H. Hietala, and V. Angelopoulos (2013), Anti-sunward high-speed jets in the subsolar magnetosheath, *Ann. Geophys.*, *31*, 1877–1889, doi:10.5194/angeo-31-1877-2013.

Rème, H., et al. (2001), First multispacecraft ion measurements in and near the Earth's magnetosphere with the identical Cluster Ion Spectrometry (CIS) experiment, *Ann. Geophys.*, *19*, 1303–1354, doi:10.5194/angeo-19-1303-2001.

Russell, C. T., and R. C. Elphic (1979), ISEE observations of flux transfer events at the dayside magnetopause, *Geophys. Res. Lett.*, *6*(1), 33–36, doi:10.1029/GL006i001p00033.

Savin, S., et al. (2008), High energy jets in the Earth's magnetosheath: Implications for plasma dynamics and anomalous transport, *JETP Lett.*, *87*, 593–599, doi:10.1134/S0021364008110015.

Savin, S., et al. (2012), Super fast plasma streams as drivers of transient and anomalous magnetospheric dynamics, *Ann. Geophys.*, *30*, 1–7, doi:10.5194/angeo-30-1-2012.

Scholer, M., and D. Burgess (1992), The role of upstream waves in supercritical quasi-parallel shock reformation, *J. Geophys. Res.*, *97*, 8319–8326.

Schwartz, S. J. (1991), Magnetic field structures and related phenomena at quasi-parallel shocks, *Adv. Space Res.*, *11*, 9231–9240.

Schwartz, S. J., and D. Burgess (1991), Quasi-parallel shocks: A patchwork of three-dimensional structures, *Geophys. Res. Lett.*, *18*, 373–376, doi:10.1029/91GL00138.

Schwartz, S. J., D. Burgess, W. P. Wilkinson, R. L. Kessel, M. Dunlop, and H. Lühr (1992), Observations of short large-amplitude magnetic structures at a quasi-parallel shock, *J. Geophys. Res.*, *97*(A4), 4209–4227, doi:10.1029/91JA02581.

Schwartz, S. J., G. Paschmann, N. Sckopke, T. M. Bauer, M. Dunlop, A. N. Fazakerley, and M. F. Thomsen (2000), Conditions for the formation of hot flow anomalies at Earth's bow shock, *J. Geophys. Res.*, *105*, 12,639–12,650, doi:10.1029/1999JA000320.

Shue, J.-H., J.-K. Chao, P. Song, J. P. McFadden, A. V. Suvorova, V. Angelopoulos, K.-H. Glassmeier, and F. Plaschke (2009), Anomalous magnetosheath flows and distorted subsolar magnetopause for radial interplanetary magnetic fields, *Geophys. Res. Lett.*, *36*, L18112, doi:10.1029/2009GL039842.

Sibeck, D. G., R. E. Lopez, and E. C. Roelof (1991), Solar wind control of the magnetopause shape, location, and motion, *J. Geophys. Res.*, *96*, 5489–5495, doi:10.1029/90JA02464.

Stevens, M. L., and J. C. Kasper (2007), A scale-free analysis of magnetic holes at 1 AU, *J. Geophys. Res.*, *112*, A05109, doi:10.1029/2006JA012116.

Trotignon, J. G., P. M. E. Décréau, J. L. Rauch, E. Le Guirriec, P. Canu, and F. Darrouzet (2003), The Whisper relaxation sounder onboard Cluster: A powerful tool for space plasma diagnosis around the Earth, *Cosmic Res.*, *41*, 369–372.

Tsubouchi, K., and H. Matsumoto (2005), Effect of upstream rotational field on the formation of magnetic depressions in a quasi-perpendicular shock downstream, *J. Geophys. Res.*, *110*, A04101, doi:10.1029/2004JA010818.

Tsurutani, B. T., J. K. Arballo, E. J. Smith, D. Southwood, and A. Balogh (1993), Large-amplitude magnetic pulses downstream of the Jovian bow shock: Ulysses observations, *Planet. Space Sci.*, *41*(11), 851–856.

Tsurutani, B. T., C. Galvan, J. K. Arballo, D. Winterhalter, R. Sakurai, E. J. Smith, B. Buti, G. S. Lakhina, and A. Balogh (2002), Relationship between discontinuities, magnetic holes, magnetic decreases, and nonlinear Alfvén waves: Ulysses observations over the solar poles, *Geophys. Res. Lett.*, *29*(11), 1528, doi:10.1029/2001GL013623.

Tsurutani, B. T., G. S. Lakhina, J. S. Pickett, F. L. Guarnieri, N. Lin, and B. E. Goldstein (2005), Nonlinear Alfvén waves, discontinuities, proton perpendicular acceleration, and magnetic holes/decreases in interplanetary space and the magnetosphere: Intermediate shocks?, *Nonlinear Processes Geophys.*, *12*, 321–336, doi:10.5194/npg-12-321-2005.

Tsurutani, B. T., G. S. Lakhina, O. P. Verkhoglyadova, E. Echer, F. L. Guarnieri, Y. Narita, and D. O. Constantinescu (2011), Magnetosheath and heliosheath mirror mode structures, interplanetary magnetic decreases, and linear magnetic decreases: Differences and distinguishing features, *J. Geophys. Res.*, *116*, A02103, doi:10.1029/2010JA015913.

Turner, J. M., L. F. Burlaga, N. F. Ness, and J. F. Lemaire (1977), Magnetic holes in the solar wind, *J. Geophys. Res.*, *82*(13), 1921–1924.

Vasquez, B. J., and J. V. Hollweg (1999), Formation of pressure balance structures and fast waves from nonlinear Alfvén waves, *J. Geophys. Res.*, *104*, 4681–4696, doi:10.1029/1998JA900090.

Winterhalter, D., M. Neugebauer, B. E. Goldstein, E. J. Smith, S. J. Bame, and A. Balogh (1994), Ulysses field and plasma observations of magnetic holes in the solar wind and their relation to mirror mode structures, *J. Geophys. Res.*, *99*(A12), 23,371–23,381, doi:10.1029/94JA01977.

Xiao, T., Q. Q. Shi, T. L. Zhang, S. Y. Fu, L. Li, Q. G. Zong, and H. Reme (2010), Cluster-C1 observations on the geometrical structure of linear magnetic holes in the solar wind at 1 AU, *Ann. Geophys.*, *28*, 1695–1702.

Xiao, T., Q. Q. Shi, A. M. Tian, W. J. Sun, H. Zhang, X. C. Shen, and A. M. Du (2014), Plasma and magnetic-field characteristics of magnetic decreases in the solar wind at 1 AU: Cluster-C1 observations, *Sol. Phys.*, *289*(8), 3175–3195.